© 2014. Published by The Company of Biologists Ltd | Development (2014) 141, 3944-3954 doi:10.1242/dev.110189

RESEARCH ARTICLE

Partial interchangeability of *Fz3* and *Fz6* in tissue polarity signaling for epithelial orientation and axon growth and guidance

Zhong L. Hua[1,*], Hao Chang[1,2,*], Yanshu Wang[1,2], Philip M. Smallwood[1,2] and Jeremy Nathans[1,2,3,4,‡]

ABSTRACT

In mammals, a set of anatomically diverse polarity processes – including axon growth and guidance, hair follicle orientation, and stereociliary bundle orientation in inner ear sensory hair cells – appear to be mechanistically related, as judged by their dependence on vertebrate homologues of core tissue polarity/planar cell polarity (PCP) genes in *Drosophila*. To explore more deeply the mechanistic similarities between different polarity processes, we have determined the extent to which frizzled 3 (*Fz3*) can rescue the hair follicle and Merkel cell polarity defects in frizzled 6-null ($Fz6^{-/-}$) mice, and, reciprocally, the extent to which *Fz6* can rescue the axon growth and guidance defects in $Fz3^{-/-}$ mice. These experiments reveal full rescue of the $Fz6^{-/-}$ phenotype by *Fz3* and partial rescue of the $Fz3^{-/-}$ phenotype by *Fz6*, implying that these two proteins are likely to act in a conserved manner in these two contexts. Stimulated by these observations, we searched for additional anatomical structures that exhibit macroscopic polarity and that might plausibly use Fz3 and/or Fz6 signaling. This search has revealed a hitherto unappreciated pattern of papillae on the dorsal surface of the tongue that depends, at least in part, on redundant signaling by Fz3 and Fz6. Taken together, these experiments provide compelling evidence for a close mechanistic relationship between multiple anatomically diverse polarity processes.

KEY WORDS: Planar cell polarity, Skin, Brain, Hair follicle, Tongue, Mouse

INTRODUCTION

Complex metazoan animals are replete with structures that exhibit a high degree of spatial order. One type of order is apparent in the orientation of polar structures relative to local anatomic landmarks and/or the body axes. The genetic dissection of this type of spatial order – referred to as tissue polarity or, more restrictively, planar cell polarity (PCP) – began 30 years ago with the discovery and characterization of a core set of genes in *Drosophila* that regulate the orientations of wing hairs and cuticular bristles (Adler, 2002; Goodrich and Strutt, 2011; Gubb and Garcia-Bellido, 1982). Subsequent work showed that these genes also control ommatidial chirality, implying a more general role in influencing vectorial processes during development (Jenny, 2010).

[1]Department of Molecular Biology and Genetics, Johns Hopkins University School of Medicine, Baltimore, MD 21205, USA. [2]The Howard Hughes Medical Institute, Johns Hopkins University School of Medicine, Baltimore, MD 21205, USA. [3]Department of Neuroscience, Johns Hopkins University School of Medicine, Baltimore, MD 21205, USA. [4]Department of Ophthalmology, Johns Hopkins University School of Medicine, Baltimore, MD 21205, USA.
*These authors contributed equally to this work

[‡]Author for correspondence (jnathans@jhmi.edu)

Received 15 March 2014; Accepted 14 August 2014

Homologues of *Drosophila* PCP genes are found in all vertebrates, with the added complexity that there are typically several homologues for each *Drosophila* gene. Targeted disruption of these genes in mice – including the genes coding for frizzled (Fz; ten family members), dishevelled (Dsh; three family members), Van Gogh-like (Vangl; two family members) and Celsr (three family members) proteins – has revealed multiple anatomic structures that appear to require polarity signaling to attain their correct orientations (Tissir and Goffinet, 2013; Wang and Nathans, 2007; Wynshaw-Boris, 2012). These include: (1) hair follicles and their associated structures in the skin; (2) stereociliary bundles on the apical faces of inner ear sensory hair cells; and (3) motile cilia in the trachea and on the walls of the cerebral ventricles that direct the vectorial movement of mucus and cerebrospinal fluid, respectively. Two processes that involve oriented cell movements – neural tube closure in mammals and the related process of convergent extension in amphibia and fish – also require core PCP gene function (Munoz-Soriano et al., 2012; Tada and Heisenberg, 2012).

In epithelia, where PCP has been most extensively studied, current evidence suggests that PCP signaling involves the assembly of asymmetric cell-surface complexes that organize the underlying cytoskeleton (Peng and Axelrod, 2012). In these complexes, Fz proteins are localized in the plasma membrane of one cell and face Vang/Vangl proteins in the plasma membrane of the neighboring cell. Importantly, PCP protein assemblies exhibit a macroscopic asymmetry: Fz proteins assemble exclusively on one side of each cell and Vang/Vangl proteins assemble exclusively on the opposite side. The multiple cadherin-domain protein Fmi/Stan/Celsr is present on both sides of the cell and forms homophilic interactions between adjacent cells that stabilize the complex. In current models of PCP signaling, a self-assembly process in which a Fz- or Vang/Vangl-containing hemi-complex on one cell promotes the assembly of the opposite type of hemi-complex on the neighboring cell is hypothesized to be the mechanism by which polarity information is created in and propagates across the epithelial sheet (Peng and Axelrod, 2012; Simons and Mlodzik, 2008).

The present work focuses on *Fz3* and *Fz6*, two mammalian Fz family members that are implicated in tissue polarity signaling. As judged by their amino acid sequences and intron-exon structures, *Fz3* and *Fz6* form a distinct branch within the mammalian Fz family tree (Fig. 1A,B). *Fz6* is expressed in the skin and hair follicles, and $Fz6^{-/-}$ mice exhibit a nearly complete randomization of hair follicle orientations at early times in skin development, a phenotype that resembles the phenotypes of PCP mutants in the *Drosophila* cuticle (Wang et al., 2006a, 2010). By contrast, *Fz3* is expressed in the developing central nervous system (CNS), and $Fz3^{-/-}$ mice exhibit multiple defects in axon growth and guidance, including: (1) the mis-routing of thalamocortical axons to an intra-thalamic trajectory; (2) the failure of corticothalamic axons to enter the internal capsule and reach the thalamus; (3) the absence of the corticospinal tract; (4) the randomization of spinal cord sensory axon trajectories after

Development (2014) 141, 3944-3954 doi:10.1242/dev.110189

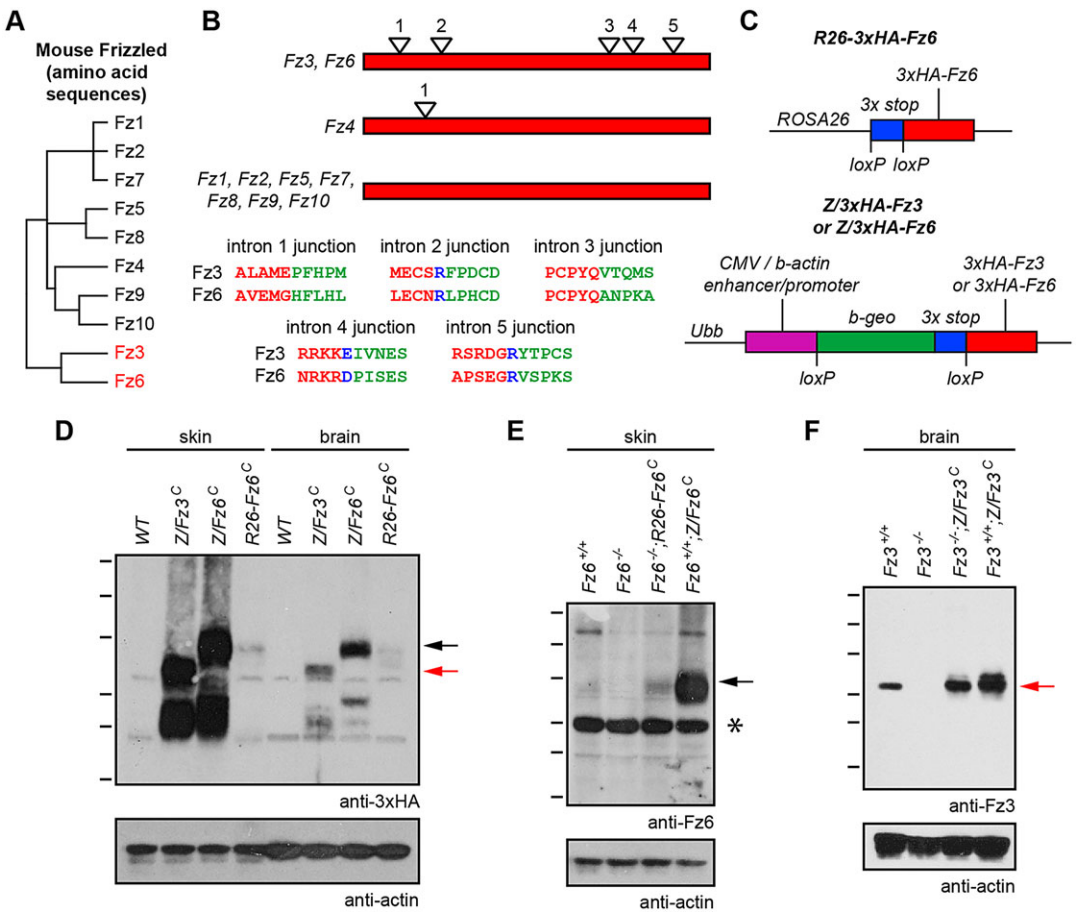

Fig. 1. Knock-in alleles for constitutive production of Fz3 and Fz6. (A) Dendrogram showing amino acid sequence identities among the 10 mouse Fz proteins. Fz3 and Fz6 show 48% amino acid identity. (B) Schematic of coding region intron-exon structures of mouse Fz family members. *Fz3* and *Fz6* each have five introns, and the intron positions are precisely conserved, as seen by the alignment of encoded amino acids near each exon-exon junction. Red lettering: amino acids encoded by the 5′ exon. Green lettering: amino acids encoded by the 3′ exon. Blue lettering: the intron is located within that codon. *Fz4* has one coding region intron; all other genes in the *Fz* family lack coding region introns. (C) Schematic of *ROSA26-3xHA-Fz6* (top), and *Z/3xHA-Fz3* and *Z/3xHA-Fz6* (bottom). At the *Z* locus, Cre-mediated deletion of the *loxP-beta-geo-stop-loxP* cassette leads to constitutive expression of *3xHA-Fz3* or *3xHA-Fz6* driven by the *CAG* promoter. At the *ROSA26* (*R26*) locus, Cre-mediated deletion of the *loxP-stop-loxP* cassette leads to constitutive expression of *3xHA-Fz6* driven by the relatively weak *ROSA26* promoter. The constitutively active derivatives of these alleles are referred to as $Z/Fz3^{C}$, $Z/Fz6^{C}$ and $R26\text{-}Fz6^{C}$, respectively. (D-F) Anti-3xHA, anti-Fz6 and anti-Fz3 immunoblots of P1 brain and skin extracts from wild-type, $Z/Fz3^{C}$, $Z/Fz6^{C}$ and $R26\text{-}Fz6^{C}$ mice in the presence or absence of endogenous *Fz3* or *Fz6* alleles, as indicated. The $Fz3^{-/-}$ brain was harvested at E18.5. The ubiquitously expressed (D) and endogenous (E) Fz6 proteins migrate at higher apparent molecular weights than the ubiquitously expressed (D) and endogenous (F) Fz3 proteins. Molecular weight (MW) heterogeneity may reflect heterogenous glycosylation. Black arrows, Fz6 protein; red arrows, Fz3 protein. Asterisk indicates an irrelevant cross-reacting band. MW standards are 180, 115, 82, 64, 49 and 37 kDa.

midline crossing; (5) the failure of some cranial motor axons to reach their muscle targets; and (6) the irreversible stalling of most hindlimb and some forelimb dorsal motor axons in the nerve plexus at the base of the limbs (Hua et al., 2013; Lyuksyutova et al., 2003; Wang et al., 2002, 2006c). Many of these defects are also seen in $Celsr3^{-/-}$ mice (Tissir et al., 2005; Zhou et al., 2008). Some of the axon guidance phenotypes observed in $Fz3^{-/-}$ mice – such as the failure of spinal cord sensory axons to turn rostrally – suggest a polarity signaling defect, whereas other phenotypes – such as the stalling of dorsal limb motor axons – do not. Evidence that Fz3 can engage the polarity signaling machinery in other contexts comes from the redundancy of *Fz3* and *Fz6* in closing the neural tube and eyelids, and in orienting inner ear sensory hair cells (Wang et al., 2006b).

The present study is aimed at determining the degree to which *Fz3* and *Fz6* are interchangeable, and, by inference, the degree to which polarity signaling in the skin and nervous system are mechanistically related. Our approach is to test whether it is possible to rescue $Fz3^{-/-}$ mice with ubiquitously expressed *Fz6* or to rescue $Fz6^{-/-}$ mice with ubiquitously expressed *Fz3*. The results show a complete phenotypic rescue of $Fz6^{-/-}$ hair patterning by *Fz3* and a partial rescue of $Fz3^{-/-}$ axon growth and guidance defects by *Fz6*. We have also searched for additional anatomic structures that exhibit macroscopic polarity to examine the contributions of *Fz3* and *Fz6* to that polarity. That search has revealed a hitherto unappreciated epithelial pattern that covers the dorsal surface of the mouse tongue and is partially disrupted by the combined loss of *Fz3* and *Fz6*.

RESULTS

Alleles for ubiquitous production of Fz3 and Fz6

To test the potential of *Fz6* to genetically rescue $Fz3^{-/-}$ mice and of *Fz3* to genetically rescue $Fz6^{-/-}$ mice, we reasoned that the simplest experimental design would be one in which the rescuing constructs were ubiquitously expressed. To this end, triple-hemaglutinin epitope (HA)-tagged Fz3- and Fz6-coding regions were inserted into the ubiquitously expressed ubiquitin B (*Ubb*) locus. The *Ubb*

Development (2014) 141, 3944-3954 doi:10.1242/dev.110189

locus is referred to hereafter as the '*Z*' locus because it is the site into which a Cre reporter transgene, *Z/AP*, was found to have randomly integrated (Lobe et al., 1999; Rotolo et al., 2008). As shown in Fig. 1C, the *Z/3xHA-Fz3* and *Z/3xHA-Fz6* knock-in alleles carry a CMV enhancer/beta-actin (*CAG*) promoter, followed by a β-galactosidase/neo ('*beta-geo*')-triple transcription stop cassette flanked by *loxP* sites (*loxP-beta-geo-stop-loxP*). In all of the experiments described here, the *loxP-beta-geo-stop-loxP* cassette was first removed by Cre-mediated recombination in the germline, generating derivatives in which the Fz3- or Fz6-coding regions were constitutively expressed, referred to as $Z/Fz3^{C}$ and $Z/Fz6^{C}$, respectively. Additionally, the 3×HA-Fz6-coding region with a triple transcription stop cassette flanked by *loxP* sites was inserted at the *ROSA26* (*R26*) locus to generate *R26-3xHA-Fz6*. Constitutive activation of this allele by germline Cre-mediated recombination generated the constitutively expressed $R26\text{-}Fz6^{C}$ allele. Expression of a single copy of $Z/Fz3^{C}$, $Z/Fz6^{C}$ or $R26\text{-}Fz6^{C}$ in a wild-type background produced no visible effect on viability, growth, fertility or overall health, implying that ubiquitous production of Fz3 or Fz6 is relatively innocuous.

Comparisons of the levels of protein production from the three ubiquitously expressed knock-in loci and from the endogenous *Fz3* and *Fz6* loci by immunoblotting show that: (1) the *CAG* promoter at the *Z* locus produces many fold higher levels of Fz3 and Fz6 than the *ROSA26* locus in both brain and skin (Fig. 1D); (2) the levels of Fz3 and Fz6 produced from the *Z* locus are higher in skin than in brain, but the levels of Fz6 produced from the *ROSA26* locus in skin and brain are more nearly equivalent (Fig. 1D); (3) the level of endogenous Fz6 in skin is barely detectable (compare $Fz6^{+/+}$ and $Fz6^{-/-}$ lanes in Fig. 1E), is several fold below the level of Fz6 produced from the *ROSA26* locus, and is many fold below the level of Fz6 produced from the *Z* locus (Fig. 1E); and (4) the level of endogenous Fz3 in brain is readily detectable and is close to the level of Fz3 produced from the *Z* locus (Fig. 1F). We note that in both brain and skin, the comparison between endogenous and ubiquitously expressed proteins does not correct for the more limited anatomic distribution of the endogenous protein, an effect that acts to minimize endogenous versus ubiquitous protein concentration differences in the relevant cell types compared with the ratios observed in the whole tissue immunoblots. For example, in the skin, endogenous *Fz6* is expressed only in the epidermis and hair follicles, whereas the *Z* and *ROSA26* loci are active in the epidermis, hair follicles, dermis and vasculature, all of which were included in the tissue homogenate.

Ubiquitous production of Fz3 rescues the $Fz6^{-/-}$ hair polarity phenotype

In the skin, *Fz6* expression – as measured with a $Fz6^{lacZ}$ knock-in allele (Guo et al., 2004) – is readily detected in the epidermis and in hair follicles, whereas *Fz3* expression – as measured with a $Fz3^{lacZ}$ knock-in allele (Wang et al., 2002) – is undetectable (Fig. 2A). Crossing $Z/Fz6^{C}$ or $R26\text{-}Fz6^{C}$ into the $Fz6^{-/-}$ background showed, as expected, a complete rescue of the $Fz6^{-/-}$ hair orientation phenotype. More interestingly, crossing $Z/Fz3^{C}$ into the $Fz6^{-/-}$ background also showed a complete rescue of the $Fz6^{-/-}$ hair orientation phenotype, as assessed on both the back and the paws

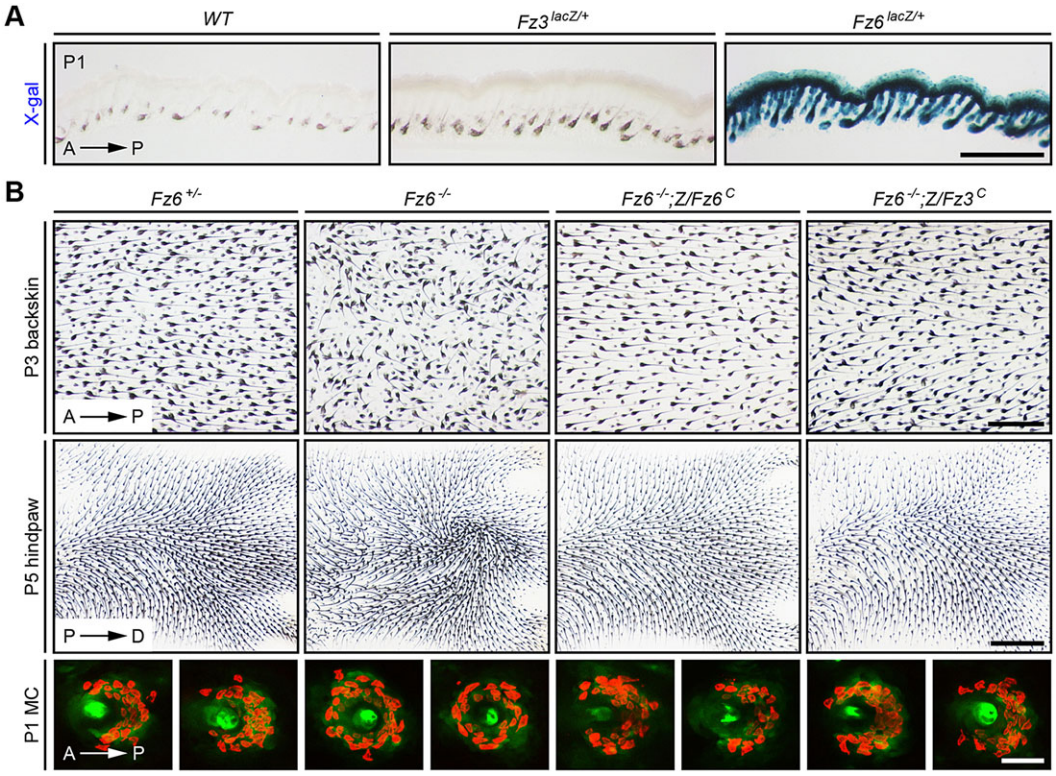

Fig. 2. Complete rescue of the $Fz6^{-/-}$ hair follicle and Merkel cell phenotypes by $Z/Fz3^{C}$. (A) X-gal staining of transverse sections of P1 back skin from $Fz6^{lacZ/+}$, $Fz3^{lacZ/+}$ and wild-type control mice. *Fz6* is expressed in epidermis and hair follicles, but *Fz3* expression is undetectable. Melanin pigmentation (brown) is visible in the follicles in each image. Similar data have been presented by Chang and Nathans (2013). Scale bar: 500 µm. (B) Upper panels show rescue of $Fz6^{-/-}$ hair follicle orientation phenotype by $Z/Fz6^{C}$ and by $Z/Fz3^{C}$ on the back [upper panels; anterior (A) is to the left and posterior (P) is to the right] and hindpaw [lower panels; proximal (P) is to the left and distal (D) is to the right]. Follicles in skin flat mounts are visualized with melanin pigment. Lower panels show rescue of $Fz6^{-/-}$ Merkel cell cluster phenotype in the back skin by $Z/Fz3^{C}$ and $Z/Fz6^{C}$ (A, anterior; P, posterior). Merkel cells are visualized with anti-cytokeratin 8 immunostaining. Scale bars: 500 µm for back skin; 1 mm for paws; 50 µm for Merkel cell clusters.

Development (2014) 141, 3944-3954 doi:10.1242/dev.110189

Table 1. Rescue of the *Fz6*$^{-/-}$ hair follicle orientation phenotype by *Z/Fz3*^{C} and *Z/Fz6*^{C}

Cross: *Fz6*$^{+/-}$;*Z/Fz6*^{C} × *Fz6*$^{-/-}$				
Progeny genotype	*Fz6*$^{-/-}$	*Fz6*$^{-/-}$;*Z/Fz6*^{C}	*Fz6*$^{+/-}$	*Fz6*$^{+/-}$;*Z/Fz6*^{C}
Wild-type phenotype	0	12	6	7
Fz6$^{-/-}$ phenotype	13	0	0	0
Cross: *Fz6*$^{+/-}$;*Z/Fz3*^{C} × *Fz6*$^{-/-}$				
Progeny genotype	*Fz6*$^{-/-}$	*Fz6*$^{-/-}$;*Z/Fz3*^{C}	*Fz6*$^{+/-}$	*Fz6*$^{+/-}$;*Z/Fz3*^{C}
Wild-type phenotype	0	9	24	14
Fz6$^{-/-}$ phenotype	18	0	0	0

(Table 1, Fig. 2B). At postnatal day (P) 3, hair follicles on the back are well oriented in an anterior-to-posterior direction in *Fz6*$^{+/-}$ mice but are severely disordered in *Fz6*$^{-/-}$ mice. In *Fz6*$^{-/-}$;*Z/Fz3*^{C} and *Fz6*$^{-/-}$;*Z/Fz6*^{C} mice, the normal anterior-to-posterior follicle orientation in back skin is restored. Similarly, at P5, hair follicles on the dorsal surface of the paws are aligned in a proximal-to-distal direction in *Fz6*$^{+/-}$ mice, whereas they form a macroscopic whorl in the center of the paws in *Fz6*$^{-/-}$ mice. In *Fz6*$^{-/-}$;*Z/Fz3*^{C} and *Fz6*$^{-/-}$;*Z/Fz6*^{C} mice, the normal proximal-to-distal follicle orientation on the paws is restored.

In wild-type mice, a semicircle of ~30 Merkel cells partially surrounds each guard hair on the back skin, with the opening of the semicircle facing anteriorly. In *Fz6*$^{-/-}$ mice, the anterior-posterior polarity of the Merkel cell cluster is lost and the Merkel cells are arranged in a complete circle (Chang and Nathans, 2013; Fig. 2B). In *Fz6*$^{-/-}$;*Z/Fz3*^{C} and *Fz6*$^{-/-}$;*Z/Fz6*^{C} mice, Merkel cell polarity is restored (Fig. 2B).

To assess the specificity of *Z/Fz3*^{C} function, we asked whether it could rescue the palate closure defect that occurs in *Fz1*$^{-/-}$;*Fz2*$^{-/-}$ embryos (Yu et al., 2010). In 9/9 *Fz1*$^{-/-}$;*Fz2*$^{-/-}$;*Z/Fz3*^{C} embryos examined, there was a failure of palate closure indistinguishable from the palate closure defect seen in *Fz1*$^{-/-}$;*Fz2*$^{-/-}$ embryos (supplementary material Fig. S1). Thus, *Z/Fz3*^{C} is capable of rescuing some Fz mutations but not others.

Ubiquitous production of Fz6 partially rescues *Fz3*$^{-/-}$ axon growth and guidance phenotypes

In the embryonic brain, *Fz3* is widely expressed (Tissir and Goffinet, 2006; Wang et al., 2002) but *Fz6* expression is largely confined to the vasculature (Z.L.H., H.C., Y.W., P.M.S. and J.N., unpublished; Daneman et al., 2009; Stenman et al., 2008). Crossing *Z/Fz3*^{C} into the *Fz3*$^{-/-}$ background showed that the neonatal lethality exhibited by *Fz3*$^{-/-}$ mice is completely rescued by ubiquitous production of Fz3 (Table 2) and, as described more fully below, the *Fz3*$^{-/-}$ axon growth and guidance phenotypes are also completely rescued (Table 3). Indeed, adult *Fz3*$^{-/-}$;*Z/Fz3*^{C} mice are healthy, fertile and indistinguishable from wild-type controls. By contrast, early postnatal lethality is not rescued in *Fz3*$^{-/-}$;*Z/Fz6*^{C} and *Fz3*$^{-/-}$;*R26-Fz6*^{C} mice (Table 2).

The failure of the *Z/Fz6*^{C} allele to rescue the *Fz3*$^{-/-}$ lethal phenotype does not necessarily imply that the *Z/Fz6*^{C} allele is without effect. To determine whether the *Z/Fz6*^{C} allele can correct some of the *Fz3*$^{-/-}$ axon growth and guidance defects, axon tracts were visualized with neurofilament (NF) immunostaining, with wild-type and *Fz3*$^{-/-}$;*Z/Fz3*^{C} embryos serving as controls (Table 3). At embryonic day (E) 11.5, the thinning of the XIIth cranial and phrenic nerves that characterizes *Fz3*$^{-/-}$ embryos (Hua et al., 2013) was rescued in both *Fz3*$^{-/-}$;*Z/Fz3*^{C} and *Fz3*$^{-/-}$;*Z/Fz6*^{C} embryos (Fig. 3A-C‴). *Fz3*$^{-/-}$;*Z/Fz6*^{C} embryos also exhibited a nearly complete rescue of the neural crest migration defect that leads to the retention of clusters of neural crest cells along the dorsal spinal cord

Table 2. *Fz3*$^{-/-}$ neonatal lethality: quantification of *Z/Fz3*^{C}, *Z/Fz6*^{C} and *R26-Fz6*^{C} rescue experiments

Postnatal survival (genotyping at adulthood)		
Cross: *Fz3*$^{+/-}$;*Z/Fz3*^{C}×*Fz3*$^{+/-}$		
Progeny genotype	*Fz3*$^{-/-}$;*Z/Fz3*^{C}	All viable progeny
Experimental data	13	76
Expected data*	11	76
Cross: *Fz3*$^{+/-}$;*Z/Fz6*^{C}×*Fz3*$^{+/-}$		
Progeny genotype	*Fz3*$^{-/-}$;*Z/Fz6*^{C}	All viable progeny
Experimental data	0	51
Expected data*	7	51
P=0.0036		
Cross: *Fz3*$^{+/-}$;*R26-Fz6*^{C}×*Fz3*$^{+/-}$		
Progeny genotype	*Fz3*$^{-/-}$;*R26-Fz6*^{C}	All viable progeny
Experimental data	0	51
Expected data*	7	51
P=0.0036		

*For each cross, one in eight mice is expected to be *Fz3*$^{-/-}$ and these die shortly after birth. The expected data are calculated for the remaining seven out of eight mice. The *P* value was calculated using a two-tailed Chi-square test.

(Fig. 3D-D‴). At E11.5, a mean of 9.5 cell clusters were seen per *Fz3*$^{-/-}$ embryo (range 7-13; *n*=4) compared with one cluster in each of two *Fz3*$^{-/-}$;*Z/Fz6*^{C} embryos and no clusters in each of three *Fz3*$^{-/-}$;*Z/Fz3*^{C} embryos.

The severe defect in thalamocortical and corticothalamic tract formation in *Fz3*$^{-/-}$ embryos was completely rescued in *Fz3*$^{-/-}$;*Z/Fz3*^{C} embryos (*n*=5), but only partially rescued in *Fz3*$^{-/-}$;*Z/Fz6*^{C} embryos (*n*=6; Fig. 4A-D′). In *Fz3*$^{-/-}$ embryos, thalamocortical and corticothalamic axons do not enter the internal capsule. In *Fz3*$^{-/-}$;*Z/Fz6*^{C} embryos, many of these axons enter the internal capsule, but the resulting tracts appear narrower (arrow in Fig. 4D) and some of the axons exhibit aberrant trajectories around the globus pallidus (arrowhead in Fig. 4D′).

Fz3$^{-/-}$;*Z/Fz6*^{C} embryos showed variable rescue of the migratory defects of VIIth cranial nerve cell bodies. In the *Fz3*$^{-/-}$ brainstem, these cells fail to migrate tangentially and caudally from rhombomere 4 to rhombomere 6, and, as a consequence, their axons fail to loop around the VIth cranial nerve nucleus (compare Fig. 4E with Fig. 4F). In *Fz3*$^{-/-}$;*Z/Fz3*^{C} embryos this defect was fully rescued (Fig. 4G). Among three *Fz3*$^{-/-}$;*Z/Fz6*^{C} embryos examined, one was completely rescued (Fig. 4H) and two showed no rescue (Fig. 4I).

In earlier work, we characterized the stalling of dorsal motor axons at the base of both fore- and hindlimbs in midgestation *Fz3*$^{-/-}$ embryos by determining the width of the dorsal nerve at different locations along its trajectory (Hua et al., 2013). Stalling is more

Table 3. *Fz3*$^{-/-}$ axon growth and guidance phenotypes: quantification of *Z/Fz3*^{C} and *Z/Fz6*^{C} rescue experiments

	Fz3$^{-/-}$;*Z/Fz3*^{C}	*Fz3*$^{-/-}$;*Z/Fz6*^{C}		
Neural development phenotype (by location)	Complete rescue	Complete rescue	Partial rescue	No rescue
Cortical/thalamic axons	5/5	0/6	6/6	0/6
VIIth nerve	1/1	1/3	0/3	2/3
XIIth nerve	3/3	6/6	0/6	0/6
Phrenic nerve	3/3	2/2	0/2	0/2
LMC_L motor nerve (forelimb)	12/12	20/20	0/20	0/20
LMC_L motor nerve (hindlimb)	5/5	12/14	0/14	2/14
Neural crest migration	3/3	0/2	2/2	0/2

Development (2014) 141, 3944-3954 doi:10.1242/dev.110189

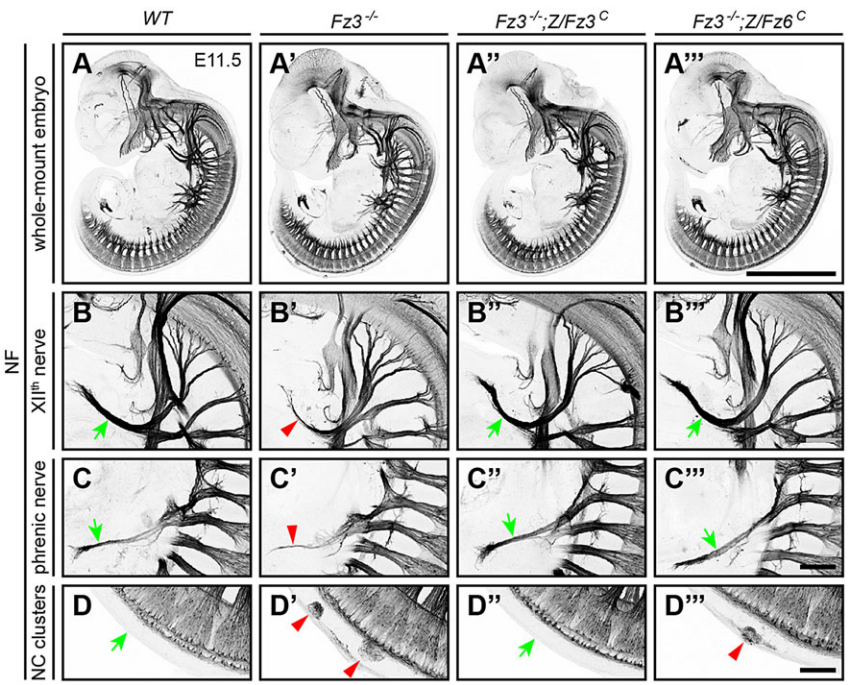

Fig. 3. Complete rescue of axon growth defect in the XIIth and phrenic nerves and partial rescue of neural crest cell migration defect in *Fz3*$^{-/-}$ embryos by *Z/Fz6*^{C}. (A-A‴) NF immunostaining of whole-mount E11.5 embryos. (B-B‴) *Fz3*$^{-/-}$ XIIth nerve is completely rescued by *Z/Fz3*^{C} and *Z/Fz6*^{C}. In *Fz3*$^{-/-}$ embryos, the XIIth nerve is markedly thinned after making a rostral turn towards the tongue (B′). (C-C‴) *Fz3*$^{-/-}$ phrenic nerve is completely rescued by *Z/Fz3*^{C} and *Z/Fz6*^{C}. In *Fz3*$^{-/-}$ embryos, the phrenic nerve is thinned (C′). (D-D‴) Neural crest cell migration defects in *Fz3*$^{-/-}$ embryos are completely rescued by *Z/Fz3*^{C} and partially rescued by *Z/Fz6*^{C}. In *Fz3*$^{-/-}$ embryos, neural crest cells that failed to migrate from the dorsal neural tube form NF-rich clusters along the caudal half of the spinal cord (A′,D′). In three *Fz3*$^{-/-}$;*Z/Fz3*^{C} embryos examined, the clusters were absent (D″). Each of two *Fz3*$^{-/-}$;*Z/Fz6*^{C} embryos examined contains one cluster (D‴). In B-D‴, green arrows show normal structures and red arrowheads show abnormal structures. Scale bars: 1 mm in A; 100 µm in B-D.

complete in the hindlimb and leads to rapid death of the corresponding motor neurons in the spinal cord. By whole-limb NF immunostaining, *Fz3*$^{-/-}$;*Z/Fz3*^{C} fore- and hindlimbs showed a complete rescue of the axon stalling defect (Table 3; Fig. 4J-L′,O-Q′; *n*=12 forelimbs and *n*=5 hindlimbs). In *Fz3*$^{-/-}$;*Z/Fz6*^{C} embryos, the forelimb phenotype was completely rescued (*n*=20 forelimbs), but a complete rescue was observed in only 12/14 hindlimbs, with the remaining 2/14 showing little or no rescue (Fig. 4M-N′,R-S′).

The complete rescue of the dorsal motor axon defect in the majority of *Fz3*$^{-/-}$ limbs by *Z/Fz6*^{C} raises the issue of whether *Fz6* normally plays any role in the development of this axon tract. To address this, we examined whole-mount limbs from E13.5 embryos in which homozygous deletion of *Fz6* in motor neurons was paired with: (1) deletion of both copies of *Fz3* (*Olig2*$^{Cre/+}$;*Fz3*$^{CKO/-}$;*Fz6*$^{-/-}$); or (2) deletion of one copy of *Fz3* (*Olig2*$^{Cre/+}$;*Fz3*$^{CKO/+}$;*Fz6*$^{-/-}$). [The use of *Olig2*^{Cre} to drive Cre-mediated recombination of *Fz3*^{CKO} avoids the potentially confounding effect of the neural tube closure defect that is part of the *Fz3*$^{-/-}$;*Fz6*$^{-/-}$ phenotype (Wang et al., 2006b).] With both *Fz3* and *Fz6* deleted (supplementary material Fig. S2C-D′,H-I′), dorsal axon thinning was indistinguishable from the *Fz3*$^{-/-}$ phenotype (supplementary material Fig. S2B,B′,G, G′; see also Fig. 4); and with one copy of *Fz3* present, loss of either one or both copies of *Fz6* did not produce any alteration in the appearance of the dorsal axon (supplementary material Fig. S2B,B′,E,E′,G,G′,J,J′). We conclude that *Fz6* has neither an independent effect on dorsal axon development nor an effect that is redundant with *Fz3*.

The complete rescue of all aspects of the *Fz3*$^{-/-}$ phenotype by *Z/Fz3*^{C}, together with the nearly identical levels of 3×HA-tagged Fz3 and Fz6 proteins produced in the brain from the *Z/Fz3*^{C} and *Z/Fz6*^{C} alleles (Fig. 1D), implies that the incomplete rescue effected by *Z/Fz6*^{C} cannot be explained by a failure of the *Z/Fz6*^{C} allele to express sufficient protein in the appropriate spatiotemporal pattern. Moreover, the rescue of the *Fz6*$^{-/-}$ skin phenotype by *Z/Fz6*^{C} and *R26-Fz6*^{C} implies that both of these knock-in alleles produce functional Fz6. The data suggest either that Fz6 is quantitatively less active in promoting axon growth and guidance than Fz3 or that Fz6 differs in some qualitative manner so that it cannot fully recapitulate Fz3 function.

Polarization of lingual papillae involves Fz3 and Fz6

The observation that Fz3 can replace Fz6 in skin PCP signaling prompted us to examine whether Fz3 might normally play a role in patterning epithelial structures. In keeping with the absence of detectable *Fz3* expression in the skin over most of the body (Fig. 2A), loss of *Fz3* did not perturb hair follicle orientation at E18.5 (supplementary material Fig. S3A,B), and the combined loss of *Fz3* and *Fz6* in the epidermis (*Fz3*$^{CKO/-}$;*Fz6*$^{-/-}$;*K14-Cre;K17-GFP*) produced a phenotype of hair follicle mis-orientation at P0 that was indistinguishable from the phenotype produced by global loss of *Fz6* (supplementary material Fig. S3C). These data imply that Fz3 plays little or no role in hair follicle orientation. [In these experiments and the ones described below, we have bypassed the CNS defects that lead to neonatal lethality in *Fz3*$^{-/-}$ mice by using a *Keratin14-Cre* (*K14-Cre*) transgene to selectively delete *Fz3* in the epidermis starting at ~E12.5-E13.5 (Beronja et al., 2010). In unpublished work we observed that *Fz6*$^{CKO/CKO}$;*K14-Cre* and *Fz6*$^{-/-}$ mice exhibit identical hair patterning phenotypes, implying that *K14-Cre* acts sufficiently early to eliminate PCP in the developing epidermis.]

In a search for other epithelial structures that exhibit large-scale polarity and that might reveal effects of Fz3 and/or cooperative effects of Fz3 and Fz6, we investigated the dorsal surface of the tongue, which in most mammals, including rodents, is covered with asymmetric epithelial protrusions (papillae). The development and micro-anatomy of lingual (i.e. tongue) papillae have been extensively studied, but their large-scale spatial organization has received little attention (Hume and Potten, 1976; Iwasaki et al., 1996). Both *Fz3* and *Fz6* are expressed in the tongue epithelium at E13.5, as judged by expression of the corresponding *lacZ* knock-in alleles (Fig. 5A). (We note that the X-gal staining intensities of these two alleles are not directly comparable: the *lacZ* knock-in at the *Fz3* locus includes an intron in the 3′ UTR and lacks a nuclear localization signal, and it is therefore likely to be a weaker reporter than the nuclear localized *lacZ* knock-in at the *Fz6* locus.)

Development (2014) 141, 3944-3954 doi:10.1242/dev.110189

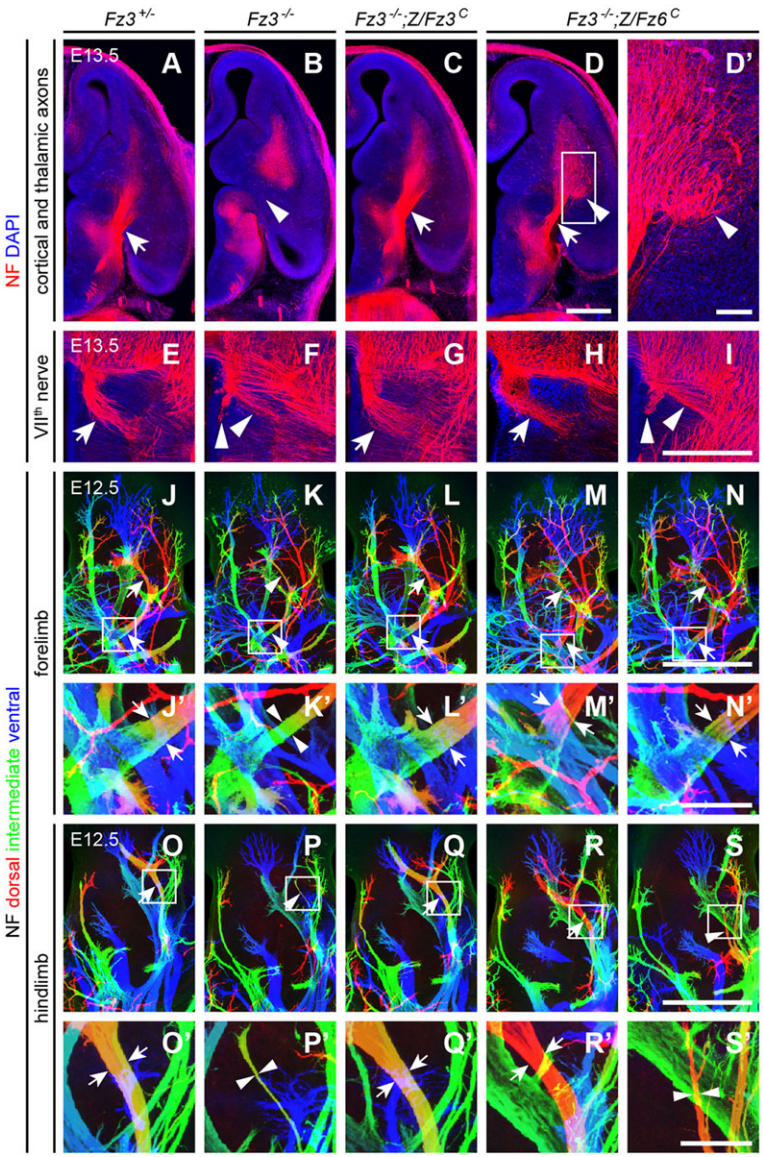

Fig. 4. Partial rescue of *Fz3*$^{-/-}$ axon growth and guidance defects in the forebrain, VIIth cranial nerve and dorsal limb motor axons by *Z/Fz6*^{C}. (A-D′) NF immunostaining of horizontal sections from E13.5 brains showing cortical and thalamic axons. The boxed region in D is enlarged in D′. Scale bars: 500 µm in D; 100 µm in D′. (E-I) NF immunostaining of horizontal sections from E13.5 brainstems showing VIIth nerve axons. Scale bar: 500 µm. (J-N′) NF immunostaining of whole-mount E13.5 forelimbs. (J′-N′) Magnified view of boxed regions in J-N. Depth within the *z*-stack along the dorsal-to-ventral axis is color-coded from red to blue. Scale bars: 500 µm in N; 100 µm in N′. (O-S′) NF immunostaining of whole-mount E13.5 hindlimbs. (O′-S′) Magnified view of boxed regions in O-S. Depth within the *z*-stack along the dorsal to ventral axis is color-coded from red to blue. Scale bars: 500 µm in S; 100 µm in S′. In A-S′, arrows show normal axon arrangements and arrowheads show abnormal arrangements.

To obtain a global assessment of the polarity of lingual papillae, we viewed the tongue as a flat-mount, using a combination of *GFP* expression from a *Keratin17-GFP* (*K17-GFP*) transgene and *in vivo* labeling with AM4-65 to assist in visualizing papillae. The wild-type mouse tongue shows a highly stereotyped pattern of papillae orientations (Fig. 5B-G). Along the front and sides, papillae make an angle of ~45° to the midline, with their raised edges pointing toward the center and posterior of the tongue. Moving more medially from each side, the papillae progressively rotate until they point posteriorly at the midline. The most distinctive feature of the papillae pattern is the presence of a single circularly symmetric rosette located at the midline ~70% of the distance from the anterior tip to the base of the tongue. The orientations of papillae at progressively greater distances from the rosette change smoothly to accommodate the vector fields at the sides and front of the tongue (Fig. 5B,F; supplementary material Fig. S4). The result is that the tongue surface exhibits two 'singularities', i.e. locations where there are large differences in the orientations of neighboring papillae. One singularity is at the center of the rosette and the second is ~1 mm anterior to the rosette, where posteriorly directed papillae from the anterior half of the tongue encounter anteriorly directed papillae from the rosette (supplementary material Fig. S4). As the entire papillae pattern is almost perfectly left-right symmetric, both singularities are located at the midline.

To determine whether Fz3 and/or Fz6 controls the patterning of lingual papillae, we examined tongues from mice missing either or both genes in the tongue epithelium at ages ranging from P3 to 9 months. As noted above in the context of supplementary material Fig. S3C, the *Fz3*^{CKO} allele was recombined with *K14-Cre*, which is expressed uniformly in the dorsal epithelium of the mature tongue, as assessed with a *Hprt-LSL-tdTomato* reporter (Wu et al., 2014; data not shown). The genotype/phenotype relationships are summarized in Table 4. In the absence of both *Fz3* and *Fz6* (*Fz3*$^{CKO/-}$;*Fz6*$^{-/-}$;*K14-Cre;K17-GFP*), the dorsal tongue surface at P20 shows no changes in the number and locations of taste buds or in the density of lingual papillae. However, papillae in the anterior half of the tongue show a general disorganization in their orientations within the plane of the tongue epithelium that is strongly reminiscent of the bristle and wing hair patterning defects observed in PCP mutants in *Drosophila* (Fig. 6C,D; Adler, 2002). In cross-sections near the midline, *Fz3*$^{CKO/-}$;*Fz6*$^{-/-}$;*K14-Cre;K17-GFP* tongues reveal numerous papillae that lack the regular anterior-to-posterior

Development (2014) 141, 3944-3954 doi:10.1242/dev.110189

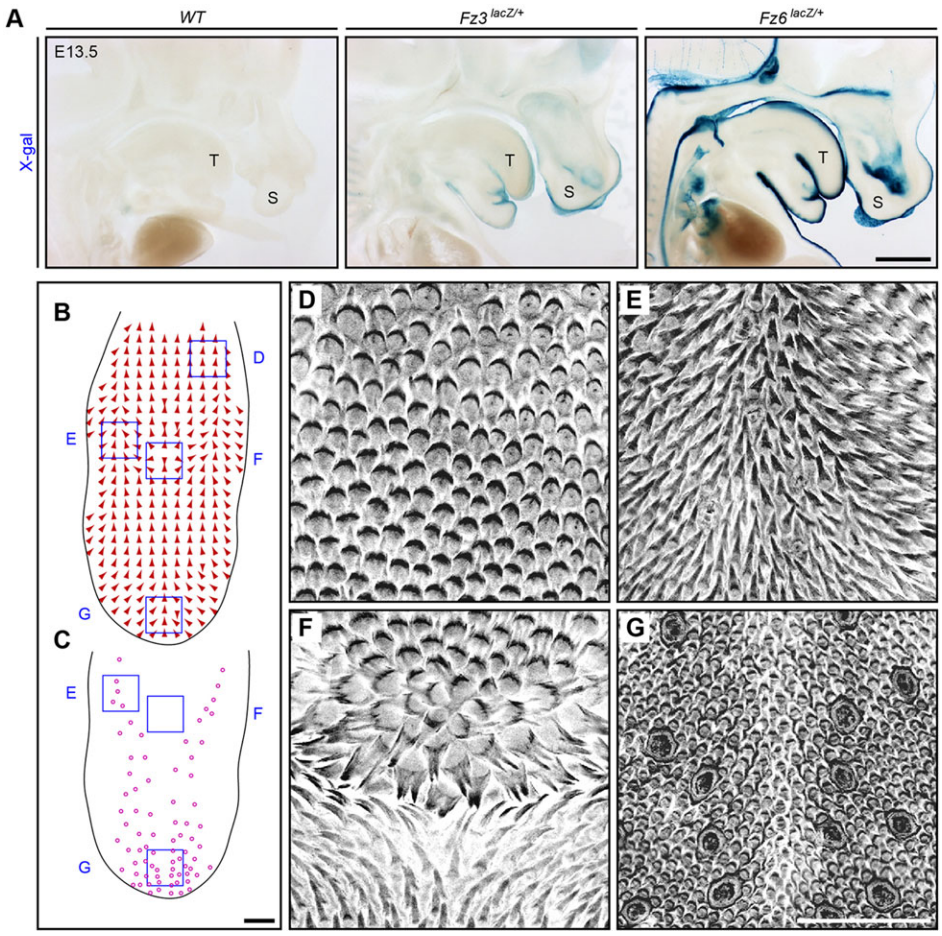

Fig. 5. Large-scale patterning of lingual papillae and expression of *Fz3* and *Fz6* in the dorsal epithelium of the wild-type mouse tongue. (A) X-gal staining of sagittal sections of E13.5 $Fz6^{lacZ/+}$, $Fz3^{lacZ/+}$ and wild-type embryos. *Fz6* is strongly expressed throughout the epidermis and in the surface epithelium of the tongue. *Fz3* is expressed in the epidermis of the snout and the surface epithelium of the tongue. Anterior is towards the right. T, tongue; S, snout. Scale bar: 1 mm. (B,C) Epithelial patterns on the dorsal surface of a wild-type tongue from a 6-month-old mouse injected with AM4-65. The global orientation of papillae (arrows) are shown in B; the locations of taste buds (circles) are shown in C. The tongue is outlined in black. Anterior is downwards. Scale bar: 1 mm. (D-G) Grayscale images of epithelial AM4-65 fluorescence correspond to the locations of the blue squares in B and C. The rosette pattern is seen in F. Anterior is downwards. Scale bar: 500 µm.

orientation observed in control tongues (Fig. 6E). By contrast, the presence of single *Fz3* allele in the absence of *Fz6* ($Fz3^{CKO/+}$;$Fz6^{-/-}$;*K14-Cre;K17-GFP*) or a single *Fz6* allele in the absence of *Fz3* ($Fz3^{CKO/-}$;$Fz6^{+/-}$;*K14-Cre;K17-GFP*) produces a papillae pattern that is indistinguishable or nearly indistinguishable from the wild type (Fig. 6A,B; supplementary material Figs S4, S5; Table 4). These data imply that *Fz3* and *Fz6* function redundantly in tongue epithelial patterning.

The localization of the patterning defect to the anterior of the tongue in $Fz3^{CKO/-}$;$Fz6^{-/-}$;*K14-Cre;K17-GFP* mice is puzzling. As lingual papillae are part of a larger integrated pattern, one might predict that any PCP gene mutations that affect lingual patterning would affect the entire pattern. Although we do not have a resolution to this apparent paradox, we speculate that if the patterning of lingual papillae roughly coincides with the time when expression of the *K14-Cre* transgene begins, and if the anterior tongue pattern develops 1-2 days later than the posterior tongue pattern or if Cre-mediated recombination occurs 1-2 days earlier in the anterior tongue, then the patterning defect in $Fz3^{CKO/-}$;$Fz6^{-/-}$;*K14-Cre;K17-GFP* mice could be limited to the anterior tongue.

Sequence divergence and evolutionary history of Fz3 and Fz6

Which domains of Fz3 and Fz6 might account for the subtly different activities of these two proteins? Alignment of mouse Fz3 and Fz6 sequences reveals a pattern of amino acid conservation that differs between domains, with 50% identity in the extracellular N-terminal cysteine-rich domain and 68% amino acid identity in the transmembrane domain, but only 23-29% identity in the cytoplasmic C-terminal tail (the range reflecting the different lengths of Fz3 and Fz6 C-terminal tails; supplementary material Fig. S6). Similar results are obtained in comparisons across other vertebrate species. Additionally, the C-terminal tails of Fz3 (169 amino acids) and Fz6 (212 amino acids) are substantially longer than the C-terminal tails of other Fz family members. The high degree of divergence between Fz3 and Fz6 in the C-terminal tail suggests that part of the activity difference between these two

Table 4. Tongue patterning phenotypes with loss of *Fz3* and/or *Fz6*

Genotype (number of *Fz3* and *Fz6* alleles)	Age	Phenotype (number of mice)
$Fz3^{+/+}$;$Fz6^{+/+}$ (4/4)	P20	WT (9)
$Fz3^{+/+}$;$Fz6^{+/+}$ (4/4)	6 months	WT (6)
$Fz3^{CKO/+}$;$Fz6^{+/-}$ (3/4)	P20	WT/M (1)
$Fz3^{CKO/+}$;$Fz6^{-/-}$ (2/4)	P20	WT (3)
$Fz3^{CKO/+}$;$Fz6^{-/-}$ (2/4)	5 months	WT (4)
$Fz3^{CKO/-}$;$Fz6^{+/-}$ (2/4)	P20	WT (2)
$Fz3^{CKO/-}$;$Fz6^{+/-}$;*K14Cre* (1/4)	P20	WT (3)
$Fz3^{CKO/+}$;$Fz6^{-/-}$;*K14Cre* (1/4)	P20	WT (1)
$Fz3^{CKO/-}$;$Fz6^{-/-}$ (1/4)	P20	WT (2)
$Fz3^{CKO/-}$;$Fz6^{-/-}$ (1/4)	P28	WT/M (1)
$Fz3^{CKO/+}$;$Fz6^{-/-}$;*K14Cre* (1/4)	5 months	WT/M (1)
$Fz3^{CKO/-}$;$Fz6^{-/-}$ (1/4)	5 months	WT (2)
$Fz3^{CKO/-}$;$Fz6^{-/-}$;*K14Cre* (0/4)	P20	M (1), M/S (1), S (3)
$Fz3^{CKO/-}$;$Fz6^{-/-}$;*K14Cre* (0/4)	5 months	M (1), S (7)
$Fz3^{CKO/-}$;$Fz6^{-/-}$;*K14Cre* (0/4)	9 months	M/S (1), S (2)

Pattern of lingual papillae: WT, wild-type pattern (Fig. 5B-G; Fig. 6A,B); M, moderately disrupted; S, severely disrupted (Fig. 6C,D). Intermediate phenotypes are indicated by WT/M or M/S.

Development (2014) 141, 3944-3954 doi:10.1242/dev.110189

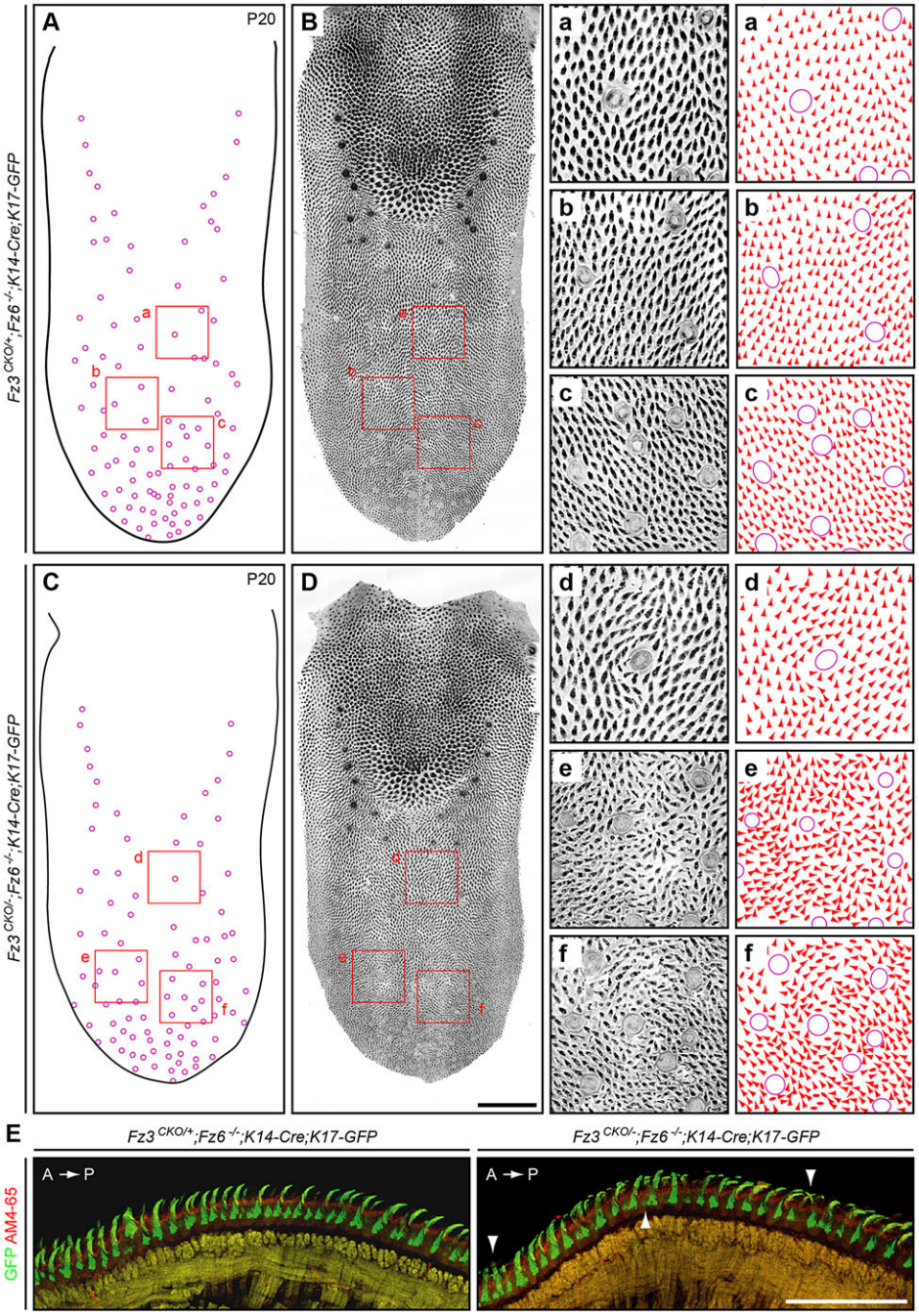

Fig. 6. Patterning of lingual papillae is partially disrupted in the anterior of the *Fz3$^{CKO/-}$;Fz6$^{-/-}$;K14-Cre* tongue. (A-D) Dorsal views of a *Fz3$^{CKO/+}$;Fz6$^{-/-}$;K14-Cre;K17-GFP* tongue (A,B) and a *Fz3$^{CKO/-}$;Fz6$^{-/-}$;K14-Cre;K17-GFP* tongue (C,D) at P20 showing the locations of taste buds (A,C) and epithelial morphology with AM4-65 and GFP fluorescence (B,D). The pattern in B matches that of wild-type tongues. Anterior is downwards. The rosette pattern is present along the midline at ~70% of the distance from the tip to the base of the tongue. The grayscale images on the right (panels a-f) correspond to the locations of the red squares in the low-magnification images on the left. The orientation of each papilla in a-f was scored with an arrowhead or, in cases where the polarity of the papillae is ambiguous, with an oval. Scale bar: 1 mm. (E) Cross-sections of the anterior dorsal surface of a control *Fz3$^{CKO/+}$;Fz6$^{-/-}$;K14-Cre;K17-GFP* tongue (left; wild-type pattern) and a *Fz3$^{CKO/-}$;Fz6$^{-/-}$;K14-Cre;K17-GFP* tongue (right) at 3 months of age. Arrowheads indicate some of the mis-oriented papillae in the right panel. The mice were injected intraperitoneally with AM4-65 1 day prior to sacrifice. A, anterior; P, posterior. Scale bar: 500 µm.

proteins in the context of CNS development may reside in this region, an idea that could be tested by swapping this domain.

Alignments of Fz amino acid sequences deduced from genomic and cDNA sequences of diverse vertebrates and invertebrates show that the Fz3/Fz6 branch within the Fz family arose in the vertebrate lineage (Fig. 7). Moreover, the division of that branch into Fz3 and Fz6 sub-branches appears to have occurred early in the vertebrate lineage, as the two sub-branches are found among all major vertebrate divisions. By contrast, the genome of *C. intestinalis*, a primitive chordate, codes for only one Fz3/Fz6-like sequence. [The identification of a *Fz3* homologue but not a *Fz6* homologue among *P. marinus* (lamprey) sequences should be interpreted cautiously, as genomic sequences from this species are substantially incomplete.] In sum, current evidence indicates that all jawed vertebrates (Gnathostomata) use distinct Fz3 and Fz6 proteins, suggesting that the division of function between these two family members occurred at least 400 million years ago.

DISCUSSION

The experiments reported here provide strong evidence that Fz3 and Fz6 have broadly similar functional properties. They also imply that the molecular mechanisms of transmembrane signaling in Fz3-mediated axon growth and guidance and in Fz6-mediated hair follicle polarity involve at least some homologous protein-protein interactions. As *Fz3* and *Fz6* homologues exist in amphibia, birds, fish and mammals, the signaling mechanisms that use their shared structural and functional motifs likely pre-date the ancestral duplication event that created separate *Fz3* and *Fz6* genes at the beginning of the vertebrate radiation. This general view is further supported by the observation that loss-of-function mutation of the

Development (2014) 141, 3944-3954 doi:10.1242/dev.110189

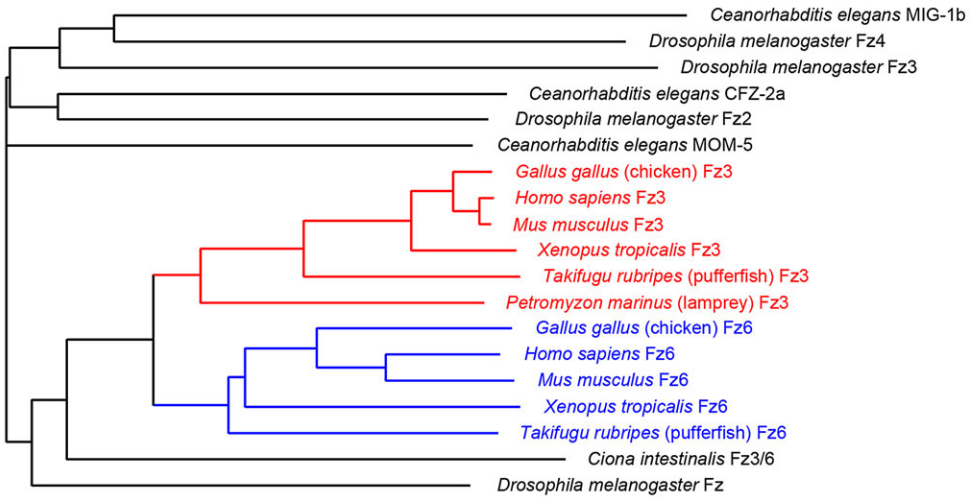

Fig. 7. Evolutionary divergence of Fz3 and Fz6 sequences. Dendrogram showing amino acid divergence of Fz3 (red) and Fz6 (blue) from select vertebrates, the closest Frizzled homologue from *Ciona intestinalis*, and all of the Frizzled family members from *C. elegans* and *D. melanogaster*. The ID numbers of the sequences used are listed in supplementary material Table S1.

core PCP gene *Celsr1* produces a hair follicle orientation phenotype closely resembling the $Fz6^{-/-}$ phenotype (Ravni et al., 2009), and, as noted in the Introduction, loss-of-function mutation of the homologous *Celsr3* gene produces an axon guidance phenotype closely resembling the $Fz3^{-/-}$ phenotype (Tissir et al., 2005). The emerging picture is one in which Celsr and Fz represent the core components of an ancient and versatile polarity signaling complex. It is not clear whether other core PCP genes, which were initially defined in the context of epithelial polarity, also play a role in axon growth and guidance.

Partial redundancy and partial interchangeability of Fz3 and Fz6

The *Fz3* and *Fz6* rescue experiments described here can be conceptualized as a genetically engineered extension of the 'experiment of nature' in which *Fz3* and *Fz6* function redundantly in the context of neural tube and eyelid closure, inner ear sensory hair cell orientation and (as shown here) patterning of lingual papillae. Because functional redundancy is predicated on spatiotemporal overlap in expression, a failure to observe redundancy in any particular context could simply reflect the absence of expression of one of the genes, as appears to be the case for *Fz3* in skin and hair follicles. In the experiments described here, we engineered ubiquitous expression of the rescuing constructs to maximize the chances of observing functional rescue, essentially creating a synthetic form of redundancy. Conveniently, it appears that ubiquitous production of Fz3 or Fz6 is not deleterious, although we cannot rule out the possibility of subtle effects. It also appears that ubiquitous production of Fz3 or Fz6 does not elicit the induction of aberrantly oriented epithelial structures of the type observed in the *Drosophila* wing and abdomen at the boundaries between clones that differ in the level of *Fz* gene expression (Adler, 2002; Struhl et al., 2012).

The contrast between the ability of ubiquitous Fz3 to fully rescue the $Fz6^{-/-}$ hair follicle orientation/epithelial polarity phenotype and the failure of ubiquitous Fz6 to fully rescue the $Fz3^{-/-}$ axon growth and guidance phenotype suggests that epithelial polarity may be the more fundamental of the two processes, whereas axon growth/guidance may represent a process for which *Fz3* has evolved subtle alterations relative to *Fz6*. The conserved nature of epithelial PCP signaling can be seen in the morphological and molecular similarities between PCP in mammalian epithelia and in the *Drosophila* cuticle and wing, both of which require *Frizzled*, *Stan/Fmi/Celsr* and *Vang/Vangl* genes, and both of which feature asymmetric PCP protein complexes (Devenport and Fuchs, 2008; Goodrich and Strutt, 2011; Wang et al., 2006b). In *Drosophila* and *C. elegans*, *Stan/Fmi/Celsr* and *Frizzled* genes have been implicated in axon guidance, branching and target selection, and *Drosophila Stan/Fmi* has been implicated in self-avoidance in sensory dendrite tiling (Huarcaya Najarro and Ackley, 2013; Lee et al., 2003; Matsubara et al., 2011; Ng, 2012; Senti et al., 2003; Steinel and Whitington, 2009). In view of the subtly different biological activities of Fz3 and Fz6 observed here, it would be interesting to investigate whether specific classes of mutations in *Drosophila Stan/Fmi* might differentially affect epidermal polarity versus axonal/dendritic pathfinding/target selection/tiling.

Evolution of PCP genes

A general issue in the study of genome evolution relates to the biochemical and evolutionary forces that determine the sizes of gene/protein families in different species and the extent of sequence divergence among family members. In some instances, the functional properties of a gene/protein family are sufficiently well understood to provide some insights into this issue; this is especially true when the relevant biochemical properties of the proteins can be defined *in vitro*. For example, the diversification of the mammalian globin family was likely driven by the advantages associated with the different oxygen affinities of embryonic, fetal and adult hemoglobins, which promote oxygen transfer from the mother to the embryo or fetus; the diversification of the vertebrate immunoglobin family was likely driven by the advantages associated with distinct binding specificities imparted by different variable regions, which increase the diversity of the immune repertoire; and the diversification of the visual pigment family was likely driven by the advantages associated with the different absorbance spectra of visual pigment receptors, which determine the wavelengths of light that can be detected, and by the advantages associated with increasing numbers of receptors, which permits a higher dimensionality in the resulting color vision. However, for many gene families, defining the relationships between sequence, function and evolutionary pressure is more challenging, especially if the encoded proteins function in multiple biological processes. Proteins in this category include, for example, myosin (over 40 family members in mammals), small GTPases (over 100 family members in mammals) and matrix metalloproteinases (over 25 family members in mammals).

Development (2014) 141, 3944-3954 doi:10.1242/dev.110189

For the gene families encoding PCP signaling proteins, the evolutionary pressures and relationships are rendered more complex by the additional involvement of some members of these protein families in canonical Wnt signaling and/or Wnt/calcium signaling. For example, *Drosophila* Fz, one of four *Drosophila* Frizzled proteins, functions in both canonical and PCP signaling (Strutt et al., 2012), as do *Drosophila* Dsh and mammalian Dvl proteins (Gao and Chen, 2010; Wynshaw-Boris, 2012). In mammals, the extent to which each of the ten Fz proteins participates in more than one signaling pathway is not clear, although current *in vivo* data are consistent with a division of labor in which some Fz proteins, such as Fz4, signal predominantly or exclusively via the canonical Wnt pathway, and others, such as Fz3 and Fz6, signal predominantly or exclusively via the PCP pathway (Wang and Nathans, 2007; Xu et al., 2004). One evolutionary force for PCP gene diversification is likely to act at the level of gene expression, as the requirements for spatially and temporally distinctive and cell type-specific patterns of expression may exert selective pressures that can only be satisfied by evolving multiple family members with distinct promoter and enhancer sequences. The success of our genetic rescue experiments based on ubiquitous production of Fz3 and Fz6 serves as a reminder that we are still largely ignorant of the role that spatiotemporal control of gene expression plays in polarity signaling.

MATERIALS AND METHODS

Mouse lines

The *Z/3xHA-Fz3*, *Z/3xHA-Fz6* and *R26-3xHA-Fz6* alleles were generated by homologous recombination in mouse embryonic stem (ES) cells using standard techniques. Targeting constructs (Fig. 1C) were electroporated into R1 mouse ES cells. Colonies were grown in medium containing G418 and ganclovir, and were screened by karyotyping and Southern blot hybridization. Positive clones were injected into C57BL/6 blastocysts to generate chimeric founders, and germline transmission was confirmed by Southern blot hybridization and PCR.

The following mouse alleles were also used: $Fz1^{-}$ and $Fz2^{-}$ (Yu et al., 2010), $Fz3^{-}$ (Wang et al., 2002), $Fz3^{CKO}$ (Hua et al., 2013), $Fz6^{-}$ (Guo et al., 2004), *Hprt-LSL-tdTomato* (Wu et al., 2014), *K14-Cre* (Dassule et al., 2000), *K17-GFP* (Bianchi et al., 2005), $Olig2^{Cre}$ (Dessaud et al., 2007) and *Sox2-Cre* (Hayashi et al., 2002). Mice were handled and housed according to the approved Institutional Animal Care and Use Committee (IACUC) protocol MO13M469 of the Johns Hopkins Medical Institutions.

Reagents and immunohistochemistry

The following primary antibodies were used for immunohistochemistry or western blotting: mouse monoclonal anti-neurofilament (165 kDa; 2H3, Developmental Studies Hybridoma Bank; 1:1000), rabbit anti-K17 (a gift from Dr Pierre Coulombe, Johns Hopkins Univeristy, Baltimore, MD, USA; 1:1000), rat mAb anti-cytokeratin8 (CK8; TROMA-1; Developmental Studies Hybridoma Bank; 1:500), rabbit anti-Fz3 and anti-Fz6 antibodies (Wang et al., 2006b; 1:1000-1:5000), and rabbit anti-3×HA (T. Rotolo and J.N., unpublished; 1:10,000). Secondary antibodies were Alexa Fluor 488 or 594 conjugated (Invitrogen; 1:500). AM4-65 was from Biotium (#70039; 20 µg per mouse).

Immunostaining was performed on: (1) vibratome sections from embryos that were immersion fixed in 4% (w/v) paraformaldehyde (PFA) dissolved in phosphate-buffered saline (PBS) (pH 7.4) at 4°C overnight, washed three times in ice-cold PBS, embedded in 3% (w/v, dissolved in PBS) low melting point agarose and sectioned at 120 µm on a vibratome; and (2) whole-mount embryos and limbs that were immersion fixed in 4% PFA at 4°C for 2 h and washed three times in ice-cold PBS.

For immunostaining of 120 µm vibratome sections, sections were blocked in PBST (PBS with 0.3% Triton X-100) containing 5% normal goat serum (NGS) at room temperature for 1 h, and incubated with primary antibody in PBST containing 5% NGS at 4°C overnight. Sections were then washed five times in PBST and incubated with secondary antibody in PBST containing 5% NGS at 4°C overnight. Finally, sections were washed five times in PBST and mounted on slides with Fluoromount-G (Southern Biotech).

For immunostaining of whole-mount embryos and limbs, samples were first incubated in Dent's Bleach [10% H_2O_2, 13.3% dimethyl sulfoxide (DMSO), 53.3% methanol] at 4°C for 24 h, washed in methanol five times, and fixed in Dent's Fix (20% DMSO, 80% methanol) at 4°C overnight. Samples were washed in PBS three times, incubated with primary antibody in blocking solution (20% DMSO, 75% PBST, 5% NGS, 0.025% sodium azide) at room temperature for 5 days to 1 week with gentle end-over-end rotation, and then washed five times in PBST. Samples were incubated with secondary antibody in blocking solution at room temperature for 2 days with gentle end-over-end rotation and then washed five times in PBST. Finally samples were dehydrated in 50% methanol/PBS and methanol, and cleared in benzyl benzoate: benzyl alcohol (BBBA) as described previously (Hua et al., 2013).

Skin whole mounts

The procedures for preparation and processing of skin whole mounts for Merkel cells immunostaining and imaging of hair follicles based on melanin content are described by Chang and Nathans (2013) and Chang et al. (2014).

Tongue dorsal surface whole mounts

To visualize the geometry of the lingual papillae, mice were injected intraperitoneally with ~10 µg AM4-65 dye 12-24 h prior to sacrifice, and the tissues were fixed either by perfusion (older mice) or immersion (embryos and early postnatal mice) in PFA/PBS. For mice younger than P20, epithelial GFP fluorescence from the K17-GFP transgene also helps to visualize the papillae. Tongues from mice between E18 and 9 months of age were processed for flat-mount imaging by cutting off the ventral half of the tongue and then trimming away most of the remaining connective tissue and muscle from the inner surface of the dorsal tongue. The final flat-mount preparation was 0.5-1 mm thick. As the tongue surface is gently curved, the pattern of papillae was most clearly visualized with a projection of the *z*-stack image.

Immunoblots

Skins and brains [E18.5 and postnatal day (P)1] were homogenized with a Polytron in 1.5 ml of ice-cold lysis buffer [50 mM Tris-HCl (pH 7.4), 50 mM NaCl and 2% Triton X-100] supplemented with protease inhibitors (Roche, complete mini cocktail tablets). The tissue homogenates were further incubated at 4°C for 1 h, followed by centrifugation at 10,000 ***g*** for 5 min at 4°C. The samples were resolved by SDS-PAGE on a 10% gel. Immunoblots were incubated at 4°C overnight in the following primary antibodies: affinity-purified rabbit anti-Fz3 and anti-Fz6 (Wang et al., 2006b); rabbit anti-3×HA (T. Rotolo and J.N., unpublished); or mouse anti-actin (Chemicon, MAB1501). The blots were incubated for 2 h at room temperature in HRP-conjugated secondary antibodies (Bio-Rad), and the immunoreactive bands were visualized with the SuperSignal West Pico Substrate (Pierce).

Microscopy and image analysis

Immunostained samples were imaged using a Zeiss LSM700 confocal microscope with Zen software. Images of whole-mount samples were acquired with a 10× air objective at 10 µm intervals in the *z* dimension, and the entire *z* stack was either collapsed using a maximum intensity projection or color-coded based on depth. BBBA-cleared embryos were positioned in custom-built metal embryo holders consisting of a shallow triangular trough (sides, 2 cm×2 cm×1 cm; depths, 1, 2, 3, or 4 mm). The trough was filled with BBBA and coverslipped during imaging.

Sequence alignments

Amino acid sequences were aligned with ClustalW (Vector NTI software). The dendrogram branch lengths are proportional to percent amino acid non-identity.

Acknowledgements

This work was supported by the Howard Hughes Medical Institute. The authors thank John Williams for assistance with genotyping, Terry Stromsky for assistance with artwork, and Alisa Mo and Amir Rattner for helpful comments on the manuscript.

Competing interests
The authors declare no competing financial interests.

Author contributions
Z.L.H., H.C., Y.W. and J.N. designed experiments; P.M.S. constructed knock-in mice; Z.L.H., H.C. and Y.W. conducted experiments; Z.L.H., H.C., Y.W. and J.N. analyzed data and wrote the paper.

Funding
This work was supported by the Howard Hughes Medical Institute. Deposited in PMC for release after 6 months.

Supplementary material
Supplementary material available online at
http://dev.biologists.org/lookup/suppl/doi:10.1242/dev.110189/-/DC1

References

Adler, P. N. (2002). Planar signaling and morphogenesis in Drosophila. *Dev. Cell* **2**, 525-535.
Beronja, S., Livshits, G., Williams, S. and Fuchs, E. (2010). Rapid functional dissection of genetic networks via tissue-specific transduction and RNAi in mouse embryos. *Nat. Med.* **16**, 821-827.
Bianchi, N., Depianto, D., McGowan, K., Gu, C. and Coulombe, P. A. (2005). Exploiting the keratin 17 gene promoter to visualize live cells in epithelial appendages of mice. *Mol. Cell. Biol.* **25**, 7249-7259.
Chang, H. and Nathans, J. (2013). Responses of hair follicle-associated structures to loss of planar cell polarity signaling. *Proc. Natl. Acad. Sci. USA* **110**, E908-E917.
Chang, H., Wang, Y., Wu, H. and Nathans, J. (2014). Flat mount imaging of mouse skin and its application to the analysis of hair follicle patterning and sensory axon morphology. *J. Vis. Exp.* e51749.
Daneman, R., Agalliu, D., Zhou, L., Kuhnert, F., Kuo, C. J. and Barres, B. A. (2009). Wnt/beta-catenin signaling is required for CNS, but not non-CNS, angiogenesis. *Proc. Natl. Acad. Sci. USA* **106**, 641-646.
Dessaud, E., Yang, L. L., Hill, K., Cox, B., Ulloa, F., Ribeiro, A., Mynett, A., Novitch, B. G. and Briscoe, J. (2007). Interpretation of the sonic hedgehog morphogen gradient by a temporal adaptation mechanism. *Nature* **450**, 717-720.
Dassule, H. R., Lewis, P., Bei, M., Maas, R. and McMahon, A. P. (2000). Sonic hedgehog regulates growth and morphogenesis of the tooth. *Development* **127**, 4775-4785
Devenport, D. and Fuchs, E. (2008). Planar polarization in embryonic epidermis orchestrates global asymmetric morphogenesis of hair follicles. *Nat. Cell Biol.* **10**, 1257-1268.
Gao, C. and Chen, Y.-G. (2010). Dishevelled: the hub of Wnt signaling. *Cell. Signal.* **22**, 717-727.
Goodrich, L. V. and Strutt, D. (2011). Principles of planar polarity in animal development. *Development* **138**, 1877-1892.
Gubb, D. and Garcia-Bellido, A. (1982). A genetic analysis of the determination of cuticular polarity during development in Drosophila melanogaster. *J. Embryol. Exp. Morphol.* **68**, 37-57.
Guo, N., Hawkins, C. and Nathans, J. (2004). Frizzled6 controls hair patterning in mice. *Proc. Natl. Acad. Sci. USA* **101**, 9277-9281.
Hayashi, S., Lewis, P., Pevny, L. and McMahon, A. P. (2002). Efficient gene modulation in mouse epiblast using a Sox2Cre transgenic mouse strain. *Gene Expr. Patterns* **2**, 93-97.
Hua, Z. L., Smallwood, P. M. and Nathans, J. (2013). Frizzled3 controls axonal development in distinct populations of cranial and spinal motor neurons. *Elife* **2**, e01482.
Huarcaya Najarro, E. and Ackley, B. D. (2013). C. elegans fmi-1/flamingo and Wnt pathway components interact genetically to control the anteroposterior neurite growth of the VD GABAergic neurons. *Dev. Biol.* **377**, 224-235.
Hume, W. J. and Potten, C. S. (1976). The ordered columnar structure of mouse filiform papillae. *J. Cell Sci.* **22**, 149-160.
Iwasaki, S., Yoshizawa, H. and Kawahara, I. (1996). Study by scanning electron microscopy of the morphogenesis of three types of lingual papilla in the mouse. *Acta Anat. (Basel)* **157**, 41-52.
Jenny, A. (2010). Planar cell polarity signaling in the Drosophila eye. *Curr. Top. Dev. Biol.* **93**, 189-227.
Lee, R. C., Clandinin, T. R., Lee, C.-H., Chen, P.-L., Meinertzhagen, I. A. and Zipursky, S. L. (2003). The protocadherin Flamingo is required for axon target selection in the Drosophila visual system. *Nat. Neurosci.* **6**, 557-563.
Lobe, C. G., Koop, K. E., Kreppner, W., Lomeli, H., Gertsenstein, M. and Nagy, A. (1999). Z/AP, a double reporter for cre-mediated recombination. *Dev. Biol.* **208**, 281-292.
Lyuksyutova, A. I., Lu, C.-C., Milanesio, N., King, L. A., Guo, N., Wang, Y., Nathans, J., Tessier-Lavigne, M. and Zou, Y. (2003). Anterior-posterior guidance of commissural axons by Wnt-frizzled signaling. *Science* **302**, 1984-1988.
Matsubara, D., Horiuchi, S.-Y., Shimono, K., Usui, T. and Uemura, T. (2011). The seven-pass transmembrane cadherin Flamingo controls dendritic self-avoidance via its binding to a LIM domain protein, Espinas, in Drosophila sensory neurons. *Genes Dev.* **25**, 1982-1996.
Munoz-Soriano, V., Belacortu, Y. and Paricio, N. (2012). Planar cell polarity signaling in collective cell movements during morphogenesis and disease. *Curr. Genomics* **13**, 609-622.
Ng, J. (2012). Wnt/PCP proteins regulate stereotyped axon branch extension in Drosophila. *Development* **139**, 165-177.
Peng, Y. and Axelrod, J. D. (2012). Asymmetric protein localization in planar cell polarity: mechanisms, puzzles, and challenges. *Curr. Top. Dev. Biol.* **101**, 33-53.
Ravni, A., Qu, Y., Goffinet, A. M. and Tissir, F. (2009). Planar cell polarity cadherin Celsr1 regulates skin hair patterning in the mouse. *J. Invest. Dermatol.* **129**, 2507-2509.
Rotolo, T., Smallwood, P. M., Williams, J. and Nathans, J. (2008). Genetically-directed, cell type-specific sparse labeling for the analysis of neuronal morphology. *PLoS ONE* **3**, e4099.
Senti, K.-A., Usui, T., Boucke, K., Greber, U., Uemura, T. and Dickson, B. J. (2003). Flamingo regulates R8 axon-axon and axon-target interactions in the Drosophila visual system. *Curr. Biol.* **13**, 828-832.
Simons, M. and Mlodzik, M. (2008). Planar cell polarity signaling: from fly development to human disease. *Annu. Rev. Genet.* **42**, 517-540.
Steinel, M. C. and Whitington, P. M. (2009). The atypical cadherin Flamingo is required for sensory axon advance beyond intermediate target cells. *Dev. Biol.* **327**, 447-457.
Stenman, J. M., Rajagopal, J., Carroll, T. J., Ishibashi, M., McMahon, J. and McMahon, A. P. (2008). Canonical Wnt signaling regulates organ-specific assembly and differentiation of CNS vasculature. *Science* **322**, 1247-1250.
Struhl, G., Casal, J. and Lawrence, P. A. (2012). Dissecting the molecular bridges that mediate the function of Frizzled in planar cell polarity. *Development* **139**, 3665-3674.
Strutt, D., Madder, D., Chaudhary, V. and Artymiuk, P. J. (2012). Structure-function dissection of the frizzled receptor in Drosophila melanogaster suggests different mechanisms of action in planar polarity and canonical Wnt signaling. *Genetics* **192**, 1295-1313.
Tada, M. and Heisenberg, C.-P. (2012). Convergent extension: using collective cell migration and cell intercalation to shape embryos. *Development* **139**, 3897-3904.
Tissir, F. and Goffinet, A. M. (2006). Expression of planar cell polarity genes during development of the mouse CNS. *Eur. J. Neurosci.* **23**, 597-607.
Tissir, F. and Goffinet, A. M. (2013). Atypical cadherins Celsr1-3 and planar cell polarity in vertebrates. *Prog. Mol. Biol. Transl. Sci.* **116**, 193-214.
Tissir, F., Bar, I., Jossin, Y., De Backer, O. and Goffinet, A. M. (2005). Protocadherin Celsr3 is crucial in axonal tract development. *Nat. Neurosci.* **8**, 451-457.
Wang, Y. and Nathans, J. (2007). Tissue/planar cell polarity in vertebrates: new insights and new questions. *Development* **134**, 647-658.
Wang, Y., Thekdi, N., Smallwood, P. M., Macke, J. P. and Nathans, J. (2002). Frizzled-3 is required for the development of major fiber tracts in the rostral CNS. *J. Neurosci.* **22**, 8563-8573.
Wang, Y., Badea, T. and Nathans, J. (2006a). Order from disorder: self-organization in mammalian hair patterning. *Proc. Natl. Acad. Sci. USA* **103**, 19800-19805.
Wang, Y., Guo, N. and Nathans, J. (2006b). The role of Frizzled3 and Frizzled6 in neural tube closure and in the planar polarity of inner-ear sensory hair cells. *J. Neurosci.* **26**, 2147-2156.
Wang, Y., Zhang, J., Mori, S. and Nathans, J. (2006c). Axonal growth and guidance defects in Frizzled3 knock-out mice: a comparison of diffusion tensor magnetic resonance imaging, neurofilament staining, and genetically directed cell labeling. *J. Neurosci.* **26**, 355-364.
Wang, Y., Chang, H. and Nathans, J. (2010). When whorls collide: the development of hair patterns in frizzled 6 mutant mice. *Development* **137**, 4091-4099.
Wu, H., Luo, J., Yu, H., Rattner, A., Mo, A., Wang, Y., Smallwood, P. M., Erlanger, B., Wheelan, S. J. and Nathans, J. (2014). Cellular resolution maps of X chromosome inactivation: implications for neural development, function, and disease. *Neuron* **81**, 103-119.
Wynshaw-Boris, A. (2012). Dishevelled: in vivo roles of a multifunctional gene family during development. *Curr. Top. Dev. Biol.* **101**, 213-235.
Xu, Q., Wang, Y., Dabdoub, A., Smallwood, P. M., Williams, J., Woods, C., Kelley, M. W., Jiang, L., Tasman, W., Zhang, K. et al. (2004). Vascular development in the retina and inner ear: control by Norrin and Frizzled-4, a high-affinity ligand-receptor pair. *Cell* **116**, 883-895.
Yu, H., Smallwood, P. M., Wang, Y., Vidaltamayo, R., Reed, R. and Nathans, J. (2010). Frizzled 1 and frizzled 2 genes function in palate, ventricular septum and neural tube closure: general implications for tissue fusion processes. *Development* **137**, 3707-3717.
Zhou, L., Bar, I., Achouri, Y., Campbell, K., De Backer, O., Hebert, J. M., Jones, K., Kessaris, N., de Rouvroit, C. L., O'Leary, D. et al. (2008). Early forebrain wiring: genetic dissection using conditional Celsr3 mutant mice. *Science* **320**, 946-949.